J. Fluid Mech. (1968), *vol.* 33, *part* 3, *pp.* 495–514
Printed in Great Britain

A theory of circulation control by slot-blowing, applied to a circular cylinder

By J. DUNHAM
National Gas Turbine Establishment, Farnborough, Hampshire

(Received 25 October 1967)

Lift can be generated on a circular cylinder with its axis normal to an air flow by blowing a sheet of air tangentially round the upper surface from a narrow slot or slots. This lift force may be estimated by matching the external inviscid flow field with separation points calculated by Spalding's unified boundary-layer theory. The theory reproduces experimental results reasonably well, except in certain special conditions fully discussed.

1. Introduction

It has long been known that the lift on a body in an air stream can be altered by controlling the boundary layer. In 1904, Prandtl demonstrated lift generation on a circular cylinder by suction on the upper surface. Boundary-layer control by blowing air through narrow tangential slots dates back to 1921, and flap-blowing systems are used in several current aircraft. The wall jet introduced through the slot re-energizes the boundary layer and delays its separation. This effect can be used to increase lift and to reduce drag, and this operation is referred to in this paper as 'circulation control' although this is a more restricted use of the term than that used by Lachmann (1961). There is an important distinction, too, between circulation control as studied here and a jet flap. Only a small amount of slot air is used in this circulation control, which in principle only re-energizes the boundary layer. A jet flap uses perhaps ten times as much air and adds a jet sheet to the inviscid flow field. A jet flap generates thrust as well as lift.

In mathematical terms, the problem of calculating the two-dimensional flow field around a cylinder or aerofoil of given shape and incidence is indeterminate until the circulation around it is specified. The circulation around an aerofoil with a sharp trailing edge is fixed by the Kutta–Joukowski condition. In the case of a rounded trailing edge, this simple condition is replaced by the generalized condition that the boundary layer on the upper surface separates at almost exactly the same pressure as does the boundary layer on the lower surface (Thwaites 1960). Therefore the circulation can be increased by delaying the separation on the upper surface. It is confirmed experimentally that the upper and lower surface separation pressures remain equal even on a circulation-controlled circular cylinder, and this provides the essential link for matching the boundary-layer calculations with the inviscid flow calculations. It will be demon-

https://doi.org/10.1017/S0022112068001473 Published online by Cambridge University Press

SharkNinja Ex. 1021
SharkNinja Inc. et al., v. Dyson Technology Limited.
IPR2024-00993
Page 1 of 20

strated that this approach leads to a practicable way of estimating the lift generated on a circular cylinder by circulation control. The same method could be used for other shapes of cylinder. It was first tried by Howarth (1935) on a 6/1 ellipse without boundary-layer control.

Cheeseman (1966, 1967) has proposed the application of circulation control to helicopter rotors. He devised a novel parkable rotor with blades of circular cross-section, on which lift would be generated by circulation control. The scope for moving the effective rear stagnation point and hence generating lift is obviously maximized by choosing a circular cylinder, though Cheeseman explained other important reasons for the choice too. The present theory was developed in the course of the parkable rotor project.

2. The flow model

Figure 1 shows the system considered. A circular cylinder with its axis normal to a uniform incident air flow has one or more narrow tangential slots S on the upper surface. Air is injected through these slots, which re-energizes the boundary layer and delays its separation until C. The whole flow field is assumed incompressible and two-dimensional, except that the flow through the slots themselves is calculated as one-dimensional compressible flow. The Reynolds number is assumed to be high enough to ensure turbulent separation, that is higher than about 3×10^5.

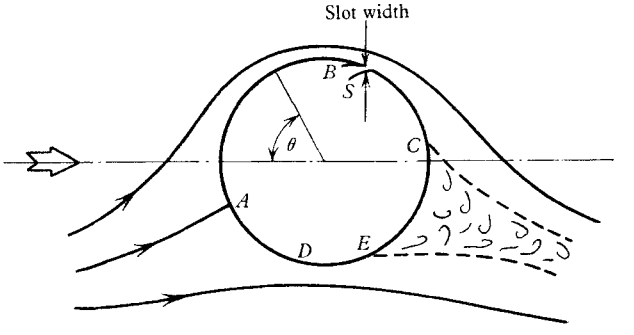

FIGURE 1. Circulation control.

The essence of the method is the step-by-step calculation of the boundary layers round the surfaces, including downstream of a slot, by the method due to Spalding (1964), until a separation criterion is satisfied. The condition that the separation velocities on the upper and lower surfaces are equal is then used.

The procedure is: (i) the lift coefficient is specified; (ii) the pressure distribution round the wetted surface is calculated from it; (iii) starting at the front stagnation point A, the laminar boundary layer is calculated step by step round the lower surface to transition at some point D; (iv) the turbulent boundary layer is then calculated step by step until a separation criterion is satisfied, at E; hence the separation pressure is found; (v) turning now to the upper surface, the laminar followed by the turbulent boundary layer is calculated step by step, including the effect of the wall jet or jets, until a separation criterion is satisfied, at C;

https://doi.org/10.1017/S0022112068001473 Published online by Cambridge University Press

SharkNinja Ex. 1021
Page 2 of 20

(vi) the strength of the wall jets is now adjusted until the upper surface separation pressure equals the previously calculated lower surface separation pressure.

This ('design') procedure gives the wall-jet strength needed to generate the specified lift coefficient. To solve the inverse ('prediction') problem—given the wall-jet strength find the lift—iterations on the 'design' procedure can be made.

Details of the individual steps are given in succeeding sections. The whole calculation has been programmed for a digital computer.

3. Theory

3.1. *Pressure distribution*

The simplest approximation to the pressure distribution on the wetted surface would be supplied by inviscid, incompressible, unseparated, potential flow theory. The flow around a circular cylinder is generated by adding a doublet to the free stream, giving

$$u = \frac{\text{velocity near surface}}{\text{free-stream velocity}} = |2\sin\theta|,$$

where θ = angle from leading edge (figure 1), and the pressure distribution is given by

$$C_p = \frac{\text{surface static pressure} - \text{free-stream static pressure}}{\text{free-stream dynamic head}}$$
$$= 1 - u^2.$$

Figure 2 shows this result in comparison with measurements by Fage & Falkner (1931) at a Reynolds number high enough to ensure turbulent separation. Any unseparated-flow theory predicts a rear stagnation point, whereas in practice the boundary layers separate from both upper and lower surfaces, leaving a region of constant pressure round the back, the 'base pressure'. Here the base pressure coefficient is $C_{pB} = -0{\cdot}52$. All the calculated pressure distributions are presented truncated at the observed base pressure in this way, ignoring the theoretical rear stagnation point and its immediate neighbourhood. It will be seen that the separated-flow or wake region is so wide that the theory gives a very poor approximation to the pressure distribution.

A source is therefore added to represent the displacement effect of the wake. If a source of arbitrary strength

$$\tfrac{1}{2}C_E \times \text{chord} \times \text{free-stream velocity}$$

is placed at what would have been the rear stagnation point, $\theta = 180°$, and also a sink of half that strength is placed at the centre of the circle, it can be shown (appendix) that no streamlines cross the surface and that

$$u = \left|2\sin\theta - \frac{C_E}{4\pi}\tan\tfrac{1}{2}\theta\right|.$$

Figure 2 also shows the pressure distribution this gives when $C_E = 3{\cdot}6$, and it agrees fairly well with the experimental points.

Because the calculated velocity distribution is truncated at the separation points, the singularity at the rear stagnation point due to the source is irrelevant.

https://doi.org/10.1017/S0022112068001473 Published online by Cambridge University Press

SharkNinja Ex. 1021
Page 3 of 20

When lift is generated, the flow model has a vortex of strength

$$\tfrac{1}{2}C_S \times \text{chord} \times \text{free-stream velocity}$$

added at the centre of the circle, and to maintain symmetry the source is moved round so as to remain at what would have been the rear stagnation point, i.e. at

$$\theta_0 = \pi - \text{front stagnation point}.$$

Then $$u = \left|2\sin\theta + \frac{C_S}{2\pi} - \frac{C_E}{4\pi}\cot\tfrac{1}{2}(\theta_0 - \theta)\right| \quad \text{(appendix)}.$$

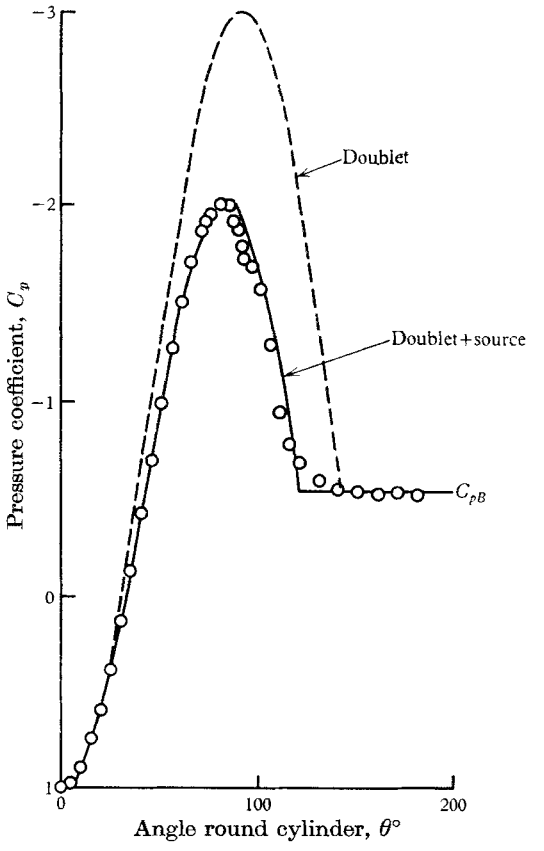

FIGURE 2. Pressure distribution at zero lift. ○, experiment, Fage & Falkner (1931).

By choice of C_E, the pressure distribution can be adjusted to fit experimental results fairly well. Figure 3 shows some pressure distributions measured by Dunham (1967) (see §5). As the lift increases the wake contracts and the need for a source diminishes; above a lift coefficient C_L of about five, simple potential flow is good enough. Figure 4 shows the variation of C_S and C_E best matching the quoted pressure distributions.

If there were no separated flow region, the lift and drag coefficients would be simply C_S and C_E respectively (hence the notation); because of the constant base

https://doi.org/10.1017/S0022112068001473 Published online by Cambridge University Press

pressure part of the surface C_S slightly exceeds C_L and C_E greatly exceeds the drag coefficient.

Inaccuracy in the assumed pressure distribution will cause an error in the calculated separation point, but the separation pressure, the important parameter, is likely to be relatively little affected.

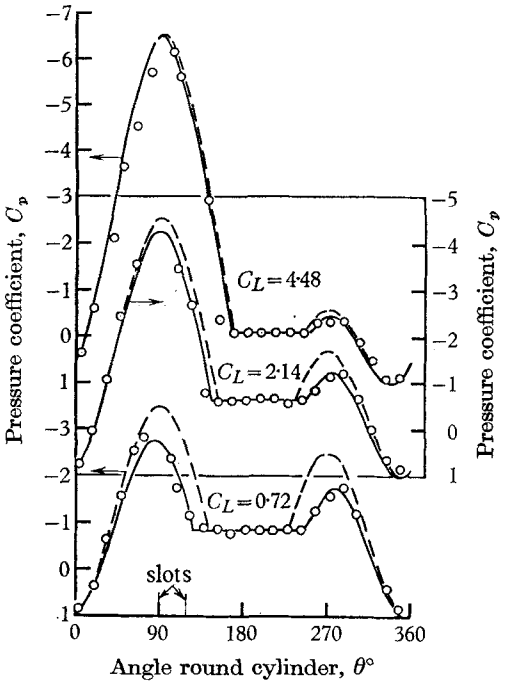

FIGURE 3. Pressure distribution. ○, experiment, Dunham (1967); — — —, doublet + vortex; ———, doublet + vortex + source.

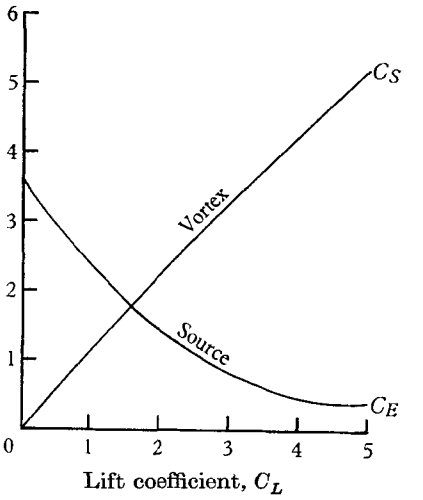

FIGURE 4. C_S and C_E required to match pressure distributions.

3.2. *Laminar boundary layer*

The method of Thwaites (1960) is used to calculate the development of the laminar boundary layer step by step from the front stagnation point to the transition point.

$$\delta = \frac{\text{momentum thickness}}{\text{chord}}$$

$$= \left(\frac{0{\cdot}45}{u^6 Re}\int_0^s u^5 ds\right)^{\frac{1}{2}},$$

where Re = Reynolds number based on chord and free-stream conditions,

s = surface distance/chord.

Transition is assumed to occur either at the first slot, or when the velocity gradient becomes adverse, whichever occurs first.

https://doi.org/10.1017/S0022112068001473 Published online by Cambridge University Press

SharkNinja Ex. 1021
Page 5 of 20

3.3. *Turbulent boundary layer*

Spalding's unified theory (Spalding 1964) is used to calculate the development of the turbulent boundary layer step by step from transition to any slots, and beyond them to separation. The essence of Spalding's velocity profile is that it embraces boundary layers with a wall jet or without one, and, alone of methods then available, can treat the decay of a wall-jet boundary layer into a normal one.

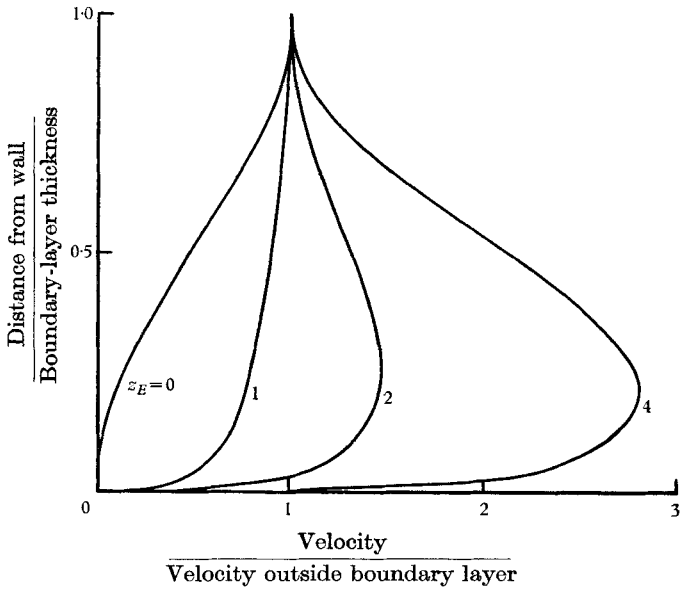

FIGURE 5. Boundary-layer velocity profiles.

Such a representation was considered essential to the present application, and was therefore adopted despite its relatively tentative status when first proposed. Spalding assumes a boundary-layer velocity profile

$$z = \frac{\text{local velocity within boundary layer}}{\text{local velocity just outside boundary layer}}$$

$$= \frac{z_E}{l}\ln\xi + z_E + \tfrac{1}{2}(1-z_E)(1-\cos\pi\xi),$$

where

$$\xi = \frac{\text{distance from wall}}{\text{boundary-layer thickness}}.$$

This is a function of two parameters, l and z_E; l can be regarded as a logarithmic Reynolds number, and z_E represents the shape of the profile. If there is a wall jet, $z_E > 1$ and is nearly proportional to the ratio of the peak wall-jet velocity to the local velocity outside the boundary layer. If there is no wall jet, $z_E < 1$ and diminishes towards separation. Figure 5 illustrates typical Spalding profiles.

The theory calculates the development of z_E, l, and a third parameter R_m, along the surface. R_m is proportional to the mass flow within the boundary layer,

https://doi.org/10.1017/S0022112068001473 Published online by Cambridge University Press

SharkNinja Ex. 1021
Page 6 of 20

and Spalding expresses the entrainment into the boundary layer by the empirical equations

$$\frac{dR_m}{ds} = 0{\cdot}06(1-z_E)uRe \quad (z_E < 1),$$
$$= 0{\cdot}03(z_E-1)uRe \quad (z_E > 1).$$

(These are the latest versions, given in the appendix to Spalding (1964).)

The boundary-layer momentum equation is

$$\frac{dz_E}{ds} = \frac{I_1(1-I_2)}{\beta}\frac{du}{ds} + \frac{I_1(I_1-I_2)}{\beta R_m}\frac{dR_m}{ds} - \frac{0{\cdot}16 I_1^2 z_E^2 uRe}{\beta l^2 R_m},$$

where

$$I_1 = \tfrac{1}{2}(1+z_E) - \frac{z_E}{l},$$

$$I_2 = 1 - \tfrac{1}{8}(1-z_E)(5+3z_E) - \frac{z_E}{l}(0{\cdot}411 + 1{\cdot}589 z_E) + \frac{2z_E^2}{l^2},$$

$$\beta = \tfrac{1}{16}(-1+6z_E+3z_E^2) + \frac{1}{l}\left(0{\cdot}1695 + \frac{2z_E}{l} - 1{\cdot}1695 z_E^2 - \frac{2z_E^2}{l^2}\right) - \frac{z_E}{l}\left(1{\cdot}589 - 2{\cdot}589\frac{z_E}{l}\right).$$

The last term of the momentum equation uses the wall friction factor

$$c_f = \frac{0{\cdot}32 z_E^2}{l^2},$$

obtained by considering the forces at the outer edge of the boundary layer.

One other equation is needed to complete the solution. This is the implicit equation relating l, z_E and R_m:

$$l = \ln\left[\frac{2{\cdot}6168 R_m z_E}{0{\cdot}5 l(1+z_E) - z_E}\right].$$

Spalding's parameters are related to the more familiar parameters of other boundary-layer theories by the equations:

$$\text{boundary-layer thickness } y_G = \left(\frac{R_m}{uI_1 Re}\right) \times \text{chord},$$
$$\text{momentum thickness } \delta_2 = (I_1 - I_2) y_G,$$
$$\text{shape factor } H = \frac{1-I_1}{I_1 - I_2}.$$

Three changes have been made by the present author before applying the theory.

The first concerns transition. The momentum thickness is assumed unchanged from the value given by Thwaites's method at the end of the laminar portion. Then z_E is assumed to be unity, so making the shape factor $H = l/(l-2)$, which takes the value 1·4 for a typical l of 7. $H = 1{\cdot}4$ is often regarded as typical after transition.

The second revision modifies Spalding's entrainment law for jet flow ($z_E > 1$) to take account of the increase in entrainment due to wall curvature. Stratford,

https://doi.org/10.1017/S0022112068001473 Published online by Cambridge University Press

SharkNinja Ex. 1021
Page 7 of 20

Jawor & Golesworthy (1962) suggested that the mixing length would be increased in the ratio

$$\left[1+2az\Big/\frac{\partial z}{\partial \xi}\right]^{-1},$$

where $$a = \frac{\text{boundary-layer thickness}}{\text{mean radius of curvature of jet centre line}}$$

and evaluated an effective mean value of $z/\partial z/\partial \xi$. This was somewhat arbitrary as $\partial z/\partial \xi \to 0$ near the edge of the boundary layer, and their final expression implied very large entrainment rates for a particular value of z_E slightly greater than unity. However, since the entrainment rate is proportional to

$$\left(\text{mixing length} \times \left|\frac{\partial z}{\partial \xi}\right|\right)^2$$

it seems better to average

$$\frac{|\partial z/\partial \xi|}{1+2az\Big/\dfrac{\partial z}{\partial \xi}} \simeq \left|\frac{\partial z}{\partial \xi}\right| + 2az,$$

which leads to an expression for entrainment uniformly applicable for all values of $z_E > 1$:

$$\frac{dR_m}{ds} = 0{\cdot}03u\,Re[(z_E-1)+2a(z_E+1)] \quad \text{(appendix)}.$$

The third change from Spalding's original method concerns separation. The success of the calculation hinges on the assessment of separation pressure. In §4.2 of his paper, Spalding introduced the pressure gradient parameter

$$F_2 = \frac{\delta_2 c}{u}\frac{du}{ds} = \frac{R_m c}{R_0}\frac{I_1-I_2}{I_1 u^2}\frac{du}{ds},$$

where c = chord,

and showed that $F_2 = -0{\cdot}004$

appeared to correlate separation points.

Later he introduced a separation criterion due to Stratford (1959) in the form

$$(F_2)_{\text{sep}} = -\left(\frac{K}{2}\right)^2 z_E^2(I_1-I_2),$$

where K is a numerical constant. For 'typical' z_E and l values, comparison between the two criteria led to $K = 0{\cdot}575$, so that the separation criterion could alternatively be written

$$\frac{F_2}{z_E^2(I_1-I_2)} = -0{\cdot}0827.$$

The original F_2 criterion cannot apply to wall-jet flow as it would never predict separation for $z_E > 1$, but the revised form can be applied to both wall-jet flow and boundary-layer flow. Sample calculations for a blown circular cylinder gave slightly different 'typical' z_E and l values, for which

$$\frac{F_2}{z_E^2(I_1-I_2)} = -0{\cdot}06$$

https://doi.org/10.1017/S0022112068001473 Published online by Cambridge University Press

fits separation better in figure 11 of Spalding (1964); furthermore, this corresponds more to the opinion of Townsend (1960) as to the value of K. This last equation is therefore used as a separation criterion on both surfaces.

3.4. *Slot flow*

The flow within a circulation control slot may be sonic or nearly sonic in many cases of practical interest even when the external flow is slow enough to justify treating it as incompressible. Therefore the slot flow is calculated on the basis of one-dimensional compressible flow theory, assuming it expands from the stagnation pressure inside the slot to the local static pressure outside the slot. If the slot is choked, the effective momentum of the wall jet is taken as the thrust on a convergent slot at that pressure ratio.

The wall-jet strength is expressed by its momentum coefficient

$$C_J = \frac{\text{wall-jet momentum}}{\text{free-stream kinetic head} \times \text{chord} \times \text{span}}.$$

This is the parameter, sometimes called C_μ, often used in studying blown flaps and jet flaps. Expressions for C_J in terms of slot width and blowing conditions are given in the appendix.

At a slot, the existing boundary layer meets the wall jet, and for perhaps six slot widths downstream the velocity profile cannot conform to Spalding's profile assumptions. There is strong entrainment in this region, and a transverse pressure gradient must be present to align the wall jet with the mainstream and the wall. The fine detail of the flow is not known, but provided separation does not occur only the subsequent values of z_E, l and R_m are of interest. If the circulation control is working as it should, separation does not occur there, so the following procedure is adopted. The mass flow in the boundary layer immediately after the slot is assumed to be the sum of the existing boundary layer mass flow plus the wall-jet flow. Similarly, the momentum in the boundary layer immediately after the slot is assumed to be the existing boundary-layer momentum plus the wall-jet momentum. These conditions suffice to define z_E, l and R_m after the slot. They probably overestimate the peak velocity in the boundary layer, but may not be unreasonable as regards entrainment and skin friction, which depend on velocity gradient.

4. Results

Figure 6 shows the computed development of the turbulent boundary layer for a typical case. The lift coefficient is 4·48, the pressure distribution is the (doublet + vortex + source) pressure distribution shown in figure 3, and the two-slot arrangement assumed was that of the model on which the experimental pressure distribution of figure 3 was observed (see §5). The calculated boundary layer on the lower surface separated at $\theta = 246{\cdot}5°$ at a base pressure coefficient of just zero, as against $-0{\cdot}1$ measured. The calculated boundary layer on the upper surface separated at the same base pressure at $\theta = 169{\cdot}7°$ provided a

https://doi.org/10.1017/S0022112068001473 Published online by Cambridge University Press

SharkNinja Ex. 1021
Page 9 of 20

momentum coefficient of 0·36 was injected (0·18 at each slot). In the corresponding experiment the momentum coefficient was in fact 0·32.

The same results are replotted in figure 7 in terms of more familiar parameters. The laminar boundary layer is also shown. In the wall-jet flow, the momentum thickness is negative and the shape factor is less than unity. The boundary-layer thickness may be compared with the slot widths of 0·024 and 0·026 in. The incoming boundary layer is 0·011 in. at the first slot and 0·057 at the second slot.

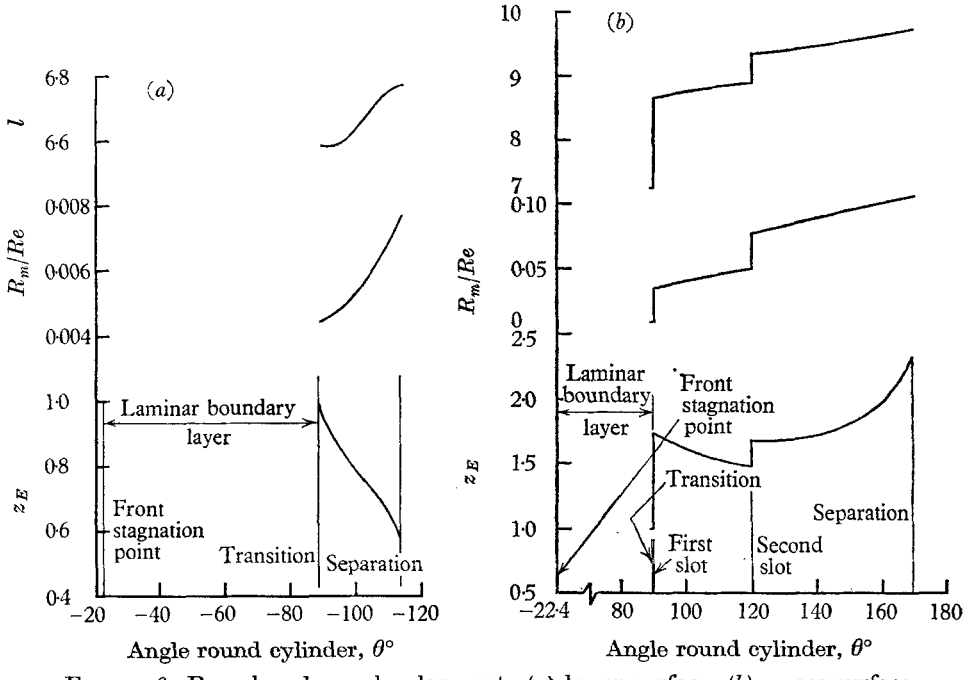

FIGURE 6. Boundary-layer development: (a) lower surface, (b) upper surface.

The theory assumes only that the incoming boundary layer and the wall jet mix as if instantaneously into a Spalding profile, without regard to their relative width, and it will become clear later that this assumption is too optimistic when the incoming boundary layer is much wider than the wall jet.

There are no measurements of boundary-layer development with which such calculations can be compared in detail. Only surface pressure distributions have been measured. Calculations can only be compared with experiments in respect of the base pressure and the lift generated by a given slot momentum. This is done for a range of slot geometry in the next section.

5. Comparison with experiments

Dunham (1967) summarized all the available experimental evidence. The number of independent variables is very large: Reynolds number, Mach number, the number of slots and their position, size and design. Examples have therefore been selected from some of the experiments to demonstrate the individual influence of these variables, and to see how well the theory reproduces the

https://doi.org/10.1017/S0022112068001473 Published online by Cambridge University Press

results. Cases have been chosen to illustrate both the strength of the theory and its weaknesses. For clarity, each experiment is identified on the graphs by a code (e.g. $R2B$); table 1 lists the test particulars for each code. All are wind-tunnel tests on two-dimensional models. Their cross-sections are reproduced in figure 8. The pressure distribution analysis (figure 3) was carried out on test $R2B$.

When the lift coefficient is known or assumed to be known, the theory calculates the base pressure by considering the lower surface only. It follows that

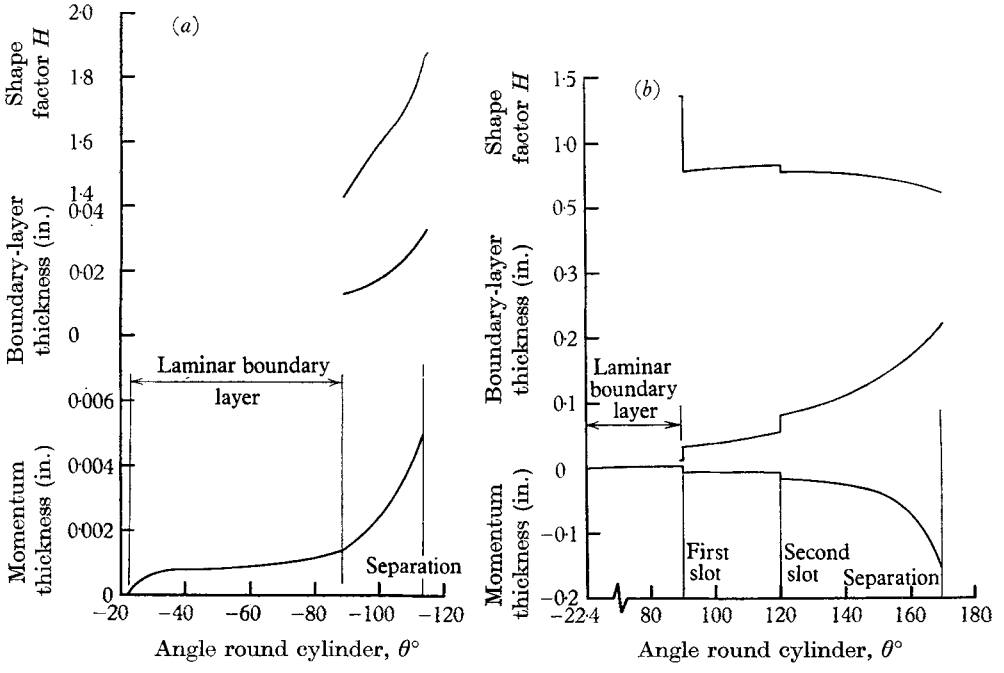

FIGURE 7. Boundary-layer development: (*a*) lower surface, (*b*) upper surface.

the base pressure coefficient is a function of lift coefficient and Reynolds number only; which slot arrangement is used to generate the lift does not affect the calculated base pressure. Measured base pressure coefficients from a wide range of tests should therefore condense to unique curves when suitably plotted. Figure 9 shows the predominant trend of results reported by Dunham (1967) at or near a Reynolds number of 360,000, at which many tests were conducted. It will be seen that in practice there is some scatter, but the theoretical curve generally agrees well with measured values.

Reynolds number can have an important influence on the flow. Below about 2×10^5 a laminar separation is found on an unblown cylinder. Above about 4×10^5 the laminar separation is followed quickly by re-attachment as a turbulent boundary layer which only separates much later. At intermediate values what happens depends on model surface condition and free-stream turbulence, and the fact that many of Dunham's tests were carried out in this transitional region must account for much of the experimental scatter. The theory does not repro-

https://doi.org/10.1017/S0022112068001473 Published online by Cambridge University Press

	Reference	Mach no.	Reynolds no.	Model details: Diameter (in.)	Span (in.)	Slot 1 (in.)	Slot 2 (in.)	Slot 1 angle θ	Slot 2 angle θ
L	*a, b*	0·11	415,000	6	24	0·006	—	90	—
$J1$	*a, c*	0·30	175,000	2	24	0·020	0·010	90	150
$J2$	*a, c*	0·16	179,000	2	24	0·020	0·010	90	150
$J3$	*a, c*	0·30	350,000	2	24	0·020	0·010	90	150
$R1$	*a*	0·31	560,000	3	24	0·003–0·007*	—	90	—
$R2A$	*a*	0·31	560,000	3	24	0·005	0·005	90	120
$R2B$	*a*	0·20	360,000	3	24	0·024	0·026	90	120
$R2C$	*a*	0·32	580,000	3	24	0·024	0·026	90	120
$R2D$	*a*	0·20	360,000	3	24	0·024	0·013	90	120
$R2E$	*a*	0·32	580,000	3	24	0·024	0·013	90	120
$R2F$	*a*	0·32	580,000	3	24	0·024	0·013	110	140
$R2G$	*a*	0·34	610,000	3	24	0·024	—	90	—
$R4$	*a*	0·32	480,000	2·5	24	0·029	—	90	—

Results from 'R' models (including figure 3) are corrected for tunnel wall interference; results from 'L' and 'J' models are uncorrected.
* This slot opened up as the slot supply pressure increased.
References: (*a*) Dunham (1967), (*b*) Lockwood (1960), (*c*) Jones & Buckingham (1964).

TABLE 1. List of experiments

http://doi.org/10.1017/S0022112068001473 Published online by Cambridge University Press

duce this effect. It is aimed at the turbulent separation condition only, so Reynolds number has a weak influence.

Mach number can be of great importance at high values, where local velocities approach or exceed the speed of sound, but the theory is essentially incompressible, and takes no account of such effects. It does, however, influence the calculations indirectly, because, when a model has more than one slot and all the slots are supplied at the same pressure, the pressure ratio across any slot is a

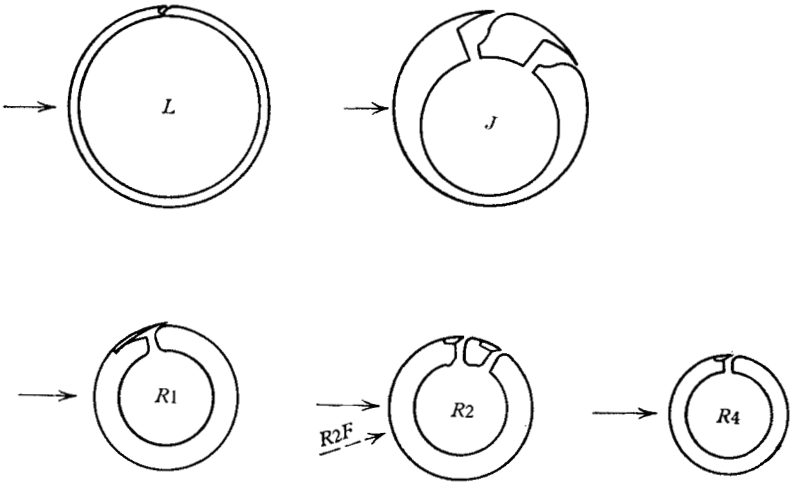

FIGURE 8. Wind-tunnel model cross-sections. Only those slots used in the tests quoted are shown.

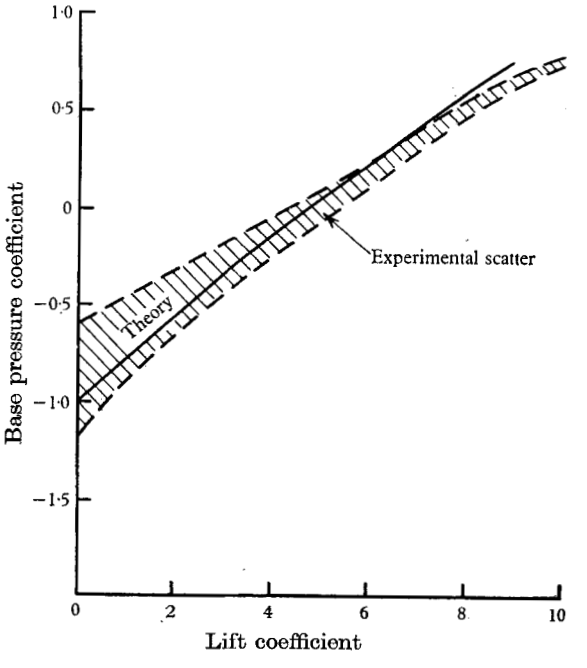

FIGURE 9. Base pressure. Reynolds number $3{\cdot}6 \times 10^5$.

https://doi.org/10.1017/S0022112068001473 Published online by Cambridge University Press

direct function of Mach number. A change of Mach number therefore alters the flow distribution between the slots, as the following example shows.

The N.G.T.E. tests were conducted at atmospheric pressure, so Reynolds number and Mach number only varied together. Jones & Buckingham (1964) however varied them independently. Figure 10*a* shows that a Mach number

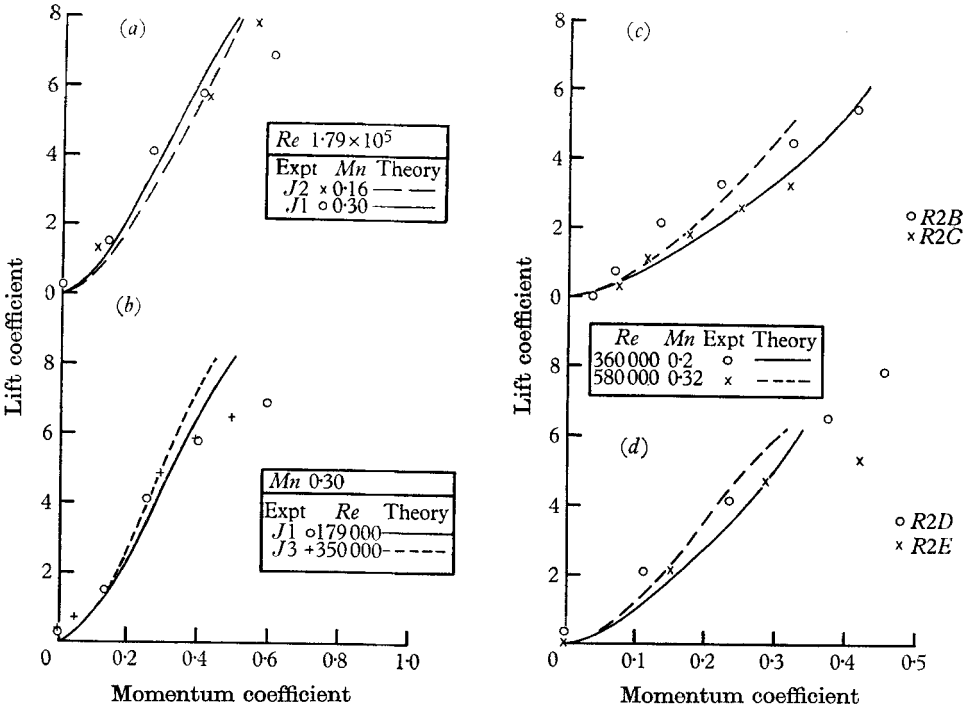

FIGURE 10. Effect of tunnel speed; (*a*) effect of Mach number at $Re = 1{\cdot}79 \times 10^5$, (*b*) effect of Reynolds number at $Mn = 0{\cdot}3$, (*c*), (*d*) changes in both Reynolds number and Mach number.

change from 0·16 to 0·30 only affected the measured lift coefficient at high lift coefficients (owing to high local Mach numbers). The difference between the theoretical calculations is that at $C_L = 4$

$$C_J = 0{\cdot}232 \text{ from slot } 1 + 0{\cdot}077 \text{ from slot } 2 \text{ at } 0{\cdot}16\ Mn.$$

$$C_J = 0{\cdot}201 \text{ from slot } 1 + 0{\cdot}077 \text{ from slot } 2 \text{ at } 0{\cdot}30\ Mn.$$

The second slot C_J is the same but as the slots were fed from a common supply the first slot took more flow at the lower Mach number. Figure 10*b* shows that Reynolds number had little influence on these tests.

Figures 10*a*, *b* also illustrate very good general agreement between calculated and measured lift coefficients up to 5.

Not all the tests were so consistent. Figures 10*c*, *d* show the effect of the same simultaneous Mach number and Reynolds number changes on two different builds of the same model in the same wind tunnel. In the lower diagram the effect was small, but in the upper diagram the lift coefficient proved much higher at the

https://doi.org/10.1017/S0022112068001473 Published online by Cambridge University Press

lower tunnel speed. The theory predicted higher lift coefficients at the higher speed in both cases and so was in fact very inaccurate at the lower speed for one of the models.

Figure 11 shows the influence of slot position. Figure 11*a* compares results on the same model at different incidences, equivalent to moving both slots simultaneously. More lift is generated when the slots are further back, and the increase

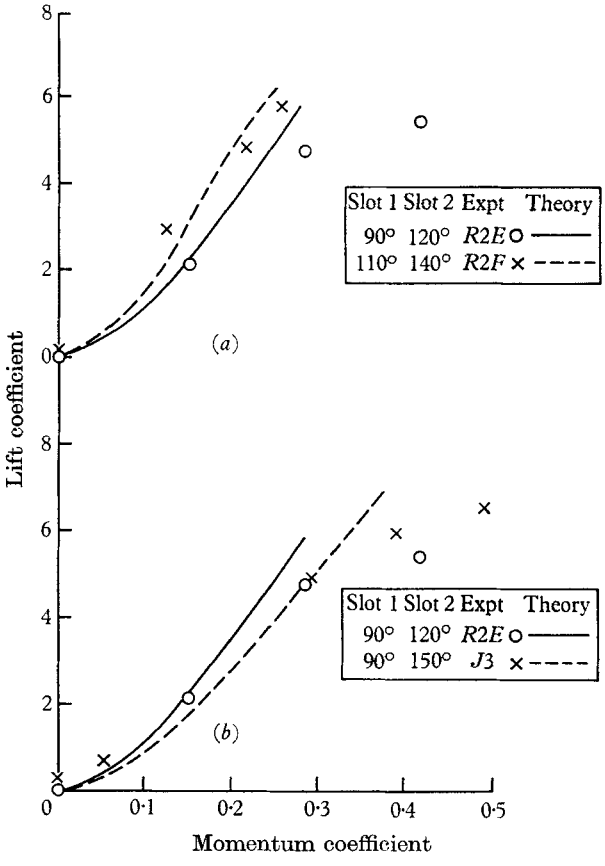

FIGURE 11. Effect of slot position, (*a*) both slots moved, (*b*) second slot only moved.

is accurately predicted. It is generally true of all tests that lift increases with incidence up to the stall (which occurs when the slots are behind the separation point) and that such increases are usually quite well predicted by the theory. Figure 11*b* shows the effect of moving only the second slot further back. The two models, tested in different wind tunnels, gave similar results, but the theory predicted a loss of lift. In general, the position of the second slot may become critical at low lift coefficients, as the slot may be after the separation point. In that event, experiments show that blowing through it can increase the lift, probably by forming a large separation bubble. The theory takes no account of this; the calculations have to assume the second-slot air expands uselessly to the base pressure. Consequently, the theory underestimates the lift generated when the second slot is too far back.

https://doi.org/10.1017/S0022112068001473 Published online by Cambridge University Press

Figure 12 illustrates the influence of slot width. In figure 12*a* the second slot has been halved in width and any given C_J generates much more lift. The increase is correctly predicted by the theory. In figure 12*b*, both slots have been reduced to only 0·005 in. The increase in lift is very marked, but not as much as the theory predicts. 0·005 in. is much smaller than the thickness of the incoming boundary layer and it seems probable that Spalding's profile family is too far removed from the true profile. The effectiveness of the wall jet is exaggerated.

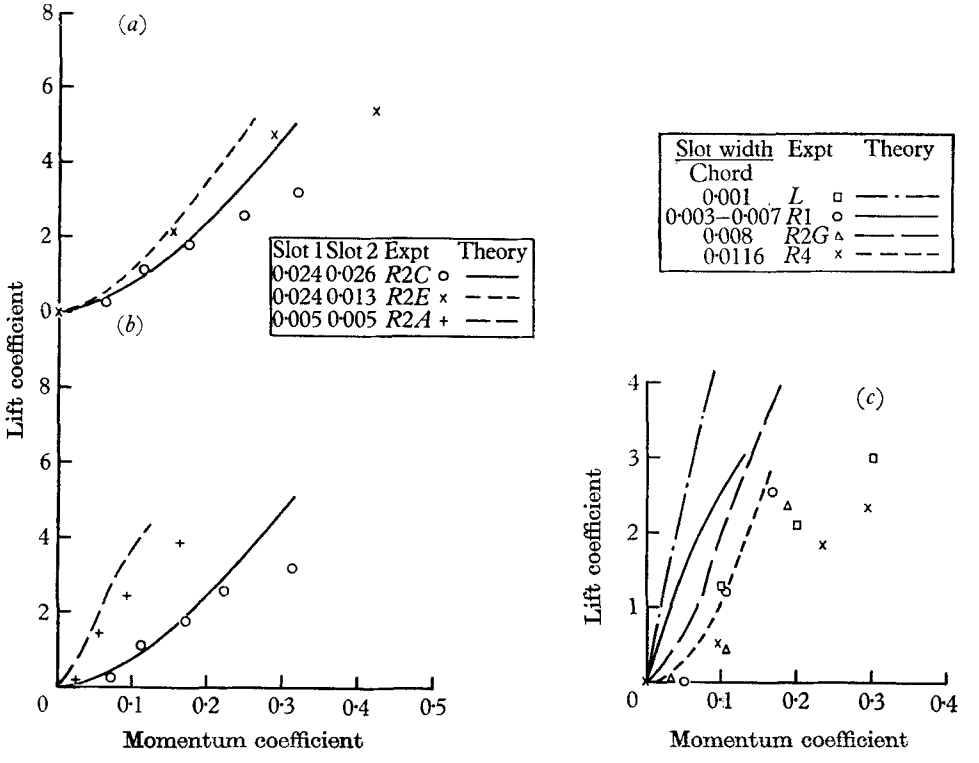

FIGURE 12. Effect of slot size, (*a*) second slot width halved, (*b*) both slots narrowed, (*c*) single-slot models.

The poor performance of a very small slot is emphasized by figure 12*c*, which shows results given by four models with single slots of widely varying sizes. The theory predicts that the smaller the slot the greater will be the lift for a given C_J. This is borne out by three of the models, but Lockwood's model with by far the smallest slot in relation to its chord gives very poor lift, only a quarter of the estimated lift. The most noticeable feature of figure 12*c*, however, is of course that all the lift coefficients are badly overestimated by the theory. This must be due to the long length of surface between the slot and separation. In a two-slot model there is a much shorter surface length between the last slot and separation for errors in the calculation of boundary-layer development to accumulate. Using Spalding's original entrainment law would about halve the estimated lift, as required; this sensitivity to the entrainment assumptions will be mentioned again.

https://doi.org/10.1017/S0022112068001473 Published online by Cambridge University Press

6. Discussion

The sensitivity of the calculations to the various numerical assumptions made was checked. The chosen step size of 2° was justified (in relation to the accuracy of the marching procedure used) by showing that a reduction to $\frac{1}{2}$° steps only altered the separation velocity by about one part in a thousand. Two changes in the transition assumptions were tried. Delaying transition until laminar separation was predicted by Thwaites's criterion (Thwaites 1960) decreased the lift by about 5 % when the first slot was at 90° but increased it by about 5 % when the first slot was at 110°; no convincing evidence was found for adopting this transition criterion generally. Changing z_E at transition by ± 10 % only changed the separation velocity by ∓ 1 % (lower surface) and $\mp 2{\cdot}8$ % (upper surface). A much more serious sensitivity was to entrainment rate. The revised entrainment law introduced in the appendix to Spalding (1964) for $z_E < 1$ only altered the separation velocity about 1 %, but the corresponding change for $z_E > 1$ resulted usually in about a 50 % increase in predicted lift, and as much as 100 % at high lift. The curvature correction is just as powerful in reducing the lift. It is not surprising that entrainment assumptions strongly influence the calculated lift. The errors in single-slot predictions and at high lift generally suggest that the entrainment rate needs to be known more accurately. The effect of changing the separation criterion from $-0{\cdot}06$ to $-0{\cdot}065$ was to increase the predicted lift by the order of 8 %. The effect of replacing calculated by measured base pressure coefficients depended, obviously, on the particular case, but did not improve accuracy significantly. There appear to be no experimental data on wall-jet separation on which to improve the criterion.

Comparison between measured and calculated lift coefficients and base pressure coefficients, both those quoted here and others, shows that the trend of results is satisfactorily predicted but that numerical accuracy is poor in some circumstances. Particular weaknesses in the theory will now be identified.

The most serious discrepancies have been encountered when the length of surface between the slots and the separation point was large, as at high lift, or when only one slot was employed. This points to the need for a more accurate entrainment law, as already discussed. There may also be a further point of principle involved. Normally, the boundary layer gets steadily 'nearer' separation in the sense that the parameter $F_2/z_E^2(I_1 - I_2)$ steadily decreases towards $-0{\cdot}06$. In some calculations at high lift, however, the parameter reached a minimum ($> -0{\cdot}06$) and then steadily increased again, taking the wall jet round the surface to the rear stagnation point. This suggests a different separation condition not now incorporated in the theory. If the last slot were much smaller than the incoming boundary layer, a free shear layer might perhaps develop and separate outside the wall jet. As already pointed out, the Spalding profile family cannot represent such a profile. This has led Professor Spalding to seek more general profiles in the later development of his theory. Similarly, difficulties in predicting entrainment have led him to adopt kinetic energy integral methods.

Failure to account for the ability of a wall jet to entrain the boundary layer

https://doi.org/10.1017/S0022112068001473 Published online by Cambridge University Press

SharkNinja Ex. 1021
Page 17 of 20

again in a bubble although it had previously separated is a defect in the formulation of the flow model, but it is not very important in this application.

Taking an overall view, the theory appears to represent most of the physical phenomena involved with reasonable quantitative accuracy. Subject to the provisos discussed, it is capable of predicting with fair accuracy the lift generated by circulation control on a circular cylinder, and is believed to be the first theory to do so.

The approach used could be applied to other shapes of body, though it is clear that where the surface radius of curvature becomes comparable with the boundary-layer thickness the boundary-layer calculation and the external potential flow calculation will react, and both may become difficult. The 'upper surface' procedure for calculating boundary-layer development to separation could be applied to flap-blowing situations more easily, because surface curvature never dominates the flow.

7. Conclusions

A theory has been developed on the basis of Spalding's unified boundary-layer theory (Spalding 1964) for calculating the wall-jet strength needed to delay boundary-layer separation until a specified point in a given pressure distribution. This has enabled estimates to be made of the lift generated on a circular cylinder with narrow tangential slots on the upper surface for boundary-layer control. Comparisons with experimentally measured lift reported by Dunham (1967) show fair numerical agreement, except when the surface distance from the last slot to the separation point is large. No boundary-layer measurements are available for detailed comparisons. The theory has been programmed for a digital computer. It could be extended to a variety of boundary-layer control applications.

Appendix

Potential flow representation

Take axes Oxy through the centre of the circle, and let the free-stream velocity be parallel to Ox. The complex velocity potential $\overline{w}$ at any point $\overline{z}$ is given by

$$\frac{\overline{w}}{U} = \overline{z} + \frac{c^2}{4\overline{z}} + \frac{icC_s}{4\pi}\ln\overline{z} + \frac{cC_E}{4\pi}\ln(\overline{z}-Z) - \frac{cC_E}{8\pi}\ln\overline{z}.$$

The velocity components v_x, v_y parallel to Ox and Oy respectively are given by putting

$$v_x - iv_y = \frac{d\overline{w}}{d\overline{z}}.$$

The surface is $x = -\frac{1}{2}c\cos\theta$, $y = \frac{1}{2}c\sin\theta$, and, if the source lies on the surface at $\theta = \theta_0$,

$$Z = -\tfrac{1}{2}c\exp(-i\theta_0).$$

The velocity components at the surface parallel and normal to it are therefore

$$\begin{aligned} v_T &= v_x\sin\theta + v_y\cos\theta \\ &= U\left[2\sin\theta + \frac{C_s}{2\pi} - \frac{C_E}{4\pi}\cot\tfrac{1}{2}(\theta_0-\theta)\right], \\ v_r &= v_y\sin\theta - v_x\cos\theta = 0. \end{aligned}$$

https://doi.org/10.1017/S0022112068001473 Published online by Cambridge University Press

Curvature correction

The average value of

$$\left|\frac{dz}{d\xi}\right| + 2az$$

over the 'outer part' of the boundary layer is approximately

$$C = \int_0^1 \left(\left|\frac{dz}{d\xi}\right| + 2az\right) d\xi$$

$$= [z]_0^1 + 2a\int_0^1 z\,d\xi.$$

Ignoring the logarithmic term which is only important between the velocity peak and the wall, the 'outer part' extends to the wall, and

$$C = z_E - 1 + a(z_E + 1).$$

In the absence of curvature

$$C = z_E - 1,$$

so the entrainment is increased in the ratio of C^2, i.e.

$$\left[1 + a\left(\frac{z_E+1}{z_E-1}\right)\right]^2 \simeq 1 + 2a\left(\frac{z_E+1}{z_E-1}\right).$$

Combining this with Spalding's formula for entrainment on a plane surface for $z_E > 1$,

$$\frac{dR_m}{ds} = 0{\cdot}03u\,Re[(z_E - 1) + 2a(z_E + 1)].$$

Momentum coefficient

The momentum coefficient is given by

$$C_J = \begin{cases} 1{\cdot}4\delta M^2 p_\infty r_\infty / qr & (M \leqslant 1), \\ 0{\cdot}74\delta p_\infty r_\infty (1{\cdot}714 - 1{\cdot}350/r)/q & (M > 1), \end{cases}$$

where δ = slot width/chord,
p = static pressure outside the slot,
p_∞ = free-stream static pressure,
$q = 0{\cdot}7M_\infty^2 p_\infty$,
M_∞ = free-stream Mach number,
M = Mach number of wall jet within slot
$= [5(r^{0{\cdot}2857} - 1)]^{\frac{1}{2}}$,
$r_\infty = P/p_\infty$,
$r = P/p$,
P = stagnation pressure of wall-jet air as supplied to the slot.

The numerical constants are for γ = ratio of specific heats = 1·4.

https://doi.org/10.1017/S0022112068001473 Published online by Cambridge University Press

SharkNinja Ex. 1021
Page 19 of 20

REFERENCES

CHEESEMAN, I. C. 1966 *Sci. J.* (September), p. 65.

CHEESEMAN, I. C. 1967 *A.I.A.A. paper* no. 67–747, 10th Anglo-American Aeronautical Conference, Los Angeles.

DUNHAM, J. 1967 Ministry of Technology Report (to be published).

FAGE, A. & FALKNER, V. M. 1931 *A.R.C. R. & M.* 1369.

HOWARTH, L. 1935 *Proc. Roy. Soc.* A **149**, 558.

JONES, A. F. & BUCKINGHAM, W. R. 1964 *A.R.C. C.P.* 889.

LACHMANN, G. V. 1961 (ed.) *Boundary Layer and Flow Control.* Oxford, Pergamon Press.

LOCKWOOD, V. E. 1960 *N.A.S.A. TN D*-244.

SPALDING, D. B. 1964 *A.R.C. C.P.* 829.

STRATFORD, B. S. 1959 *J. Fluid Mech.* **5**, 17.

STRATFORD, B. S., JAWOR, Z. M. & GOLESWORTHY, G. T. 1962 *A.R.C. C.P.* 687.

THWAITES, B. 1960 (ed.) *Incompressible Aerodynamics.* Oxford: Clarendon Press.

TOWNSEND, A. A. 1960 *J. Fluid Mech.* **8**, 143.

https://doi.org/10.1017/S0022112068001473 Published online by Cambridge University Press